The Capture Envelope of a Flanged Circular Hood in Cross Drafts

AUTHORS
Rong Fung Huang[a]
Jung Ling Chen[a]
Yu-Kang Chen[b]
Chih-Chieh Chen[c]
Wen-Yu Yeh[d]
Chun-Wann Chen[d]

[a]Department of Mechanical Engineering, National Taiwan University of Science and Technology, 43 Keelung Road, Section 4, Taipei, Taiwan; E-Mail: rfhuang@mail.ntust.edu.tw;
[b]Department of Occupational Safety and Hygiene, Chang Jung Christian University, Kway Jen, Taiwan;
[c]Institute of Occupational Medicine and Industrial Hygiene, National Taiwan University, 1 Jen-Ai Rd., Sec. 1, Taipei, Taiwan;
[d]Institute of Occupational Safety and Health, Council of Labor Affairs, 132 Min-Sheng E. Road, Taipei, Taiwan

This research was supported by the Institute of Occupational Safety and Health, Council of Labor Affairs of Taiwan.

The flow patterns of an exterior circular hood subject to the influence of various uniform cross drafts were experimentally studied in an apparatus consisting of hood-model/wind-tunnel assembly. A two-component laser Doppler anemometer was employed to measure the velocity field on the symmetry plane. The streamline patterns were obtained from the measured velocity data. The cross draft caused a characteristic envelope similar to a half Rankine body-of-revolution to form in the flow field. The boundary of the envelope is described by a dividing streamline. All streamlines within the envelope lead to the opening; those outside the envelope evolve to the downstream area. The normalized geometry of the capture envelope is theoretically justified and correlated by modifying the potential theory of point-sink-plus-rectilinear-flow. The domain and shape of the envelope enclosing the hood opening are determined primarily by the velocity ratio between the cross draft and hood suction. The correlated formula is applicable to design the hood parameters, including the sizes of opening and flange as well as the location of contaminant sources.

Keywords: capture envelope, cross draft, hood, limiting trajectory

The exterior hood has been extensively used as a local exhaust device to capture a variety of contaminants generated in a work site. In general, the exterior hood operated in a quiescent environment forms a bell-shaped capture zone.[1,2] The performance of the hood depends on how large the bell-shaped capture zone can extend to conduct an effective capture. In practical use, however, the performance of an exhaust hood is usually subject to the influences of various environmental disturbances, such as drafts from open windows or doors, cooling air currents, moving persons or objects, blockage, and so forth. Mostly, the shape and size of the bell-shaped capture zone alter significantly when the environmental disturbances apply, which usually leads to a breakdown in hood performance.

It has been theorized[3–7] that the capture zone of an exterior hood in the presence of a uniform cross draft presents an envelope with a contour similar to a half Rankine body-of-revolution[8,9] instead of a bell shape. A Rankine body-of-revolution is an axisymmetric contour with a "bomb-nose" leading edge and an infinite extension in the other end. A half Rankine body-of-revolution is formed by cutting the symmetry plane of the full body. The suction opening of the hood is enclosed in the envelope of the half Rankine body-of-revolution so that all streamlines within the envelope lead to the opening; those outside the envelope evolve to the downstream area. A contaminant outside the envelope tends to escape from the capturing of exhaust opening if the dispersion effect is ignored.[4] A cross draft drastically alters the shape and the extent of the effective capture zone so that the contaminant sources originally placed under the hood may go beyond the effective capture envelope. The physical situation is similar to the case of the aspiration of air from a moving free stream into an aerosol sampler.[10]

Chen et al.[11] and Alenius[12] employed a modified potential flow theory to calculate the flow field of a finite-opening circular hood subject to the influence of a cross draft. They obtained a limiting trajectory describing the outer boundary of a capture envelope. With the calculated limiting trajectory, the hood capacity and control velocity are derived. However, systematic experimental verification and investigation are rare in the literature. The criteria for the primary parameters of hood design and proper location of contaminant sources is still unclear.

Nomenclature

A	area of hood opening ($\pi D^2/4$)
a	radius of hood opening, 5 cm
D	diameter of hood opening, 10 cm
Q_s	volumetric suction rate of exhaust hood
R	cross draft to hood suction velocity ratio ($= V_c/V_s$)
Re_c	Reynolds number of cross draft based on hood diameter ($= V_cD/\nu$)
Re_s	Reynolds number of suction flow based on hood diameter ($= V_sD/\nu$)
V_c	velocity of cross draft
V_s	averaged suction velocity of exhaust hood ($= Q_s/A$)
W	width of flange, 30 cm
x	coordinate along hood center line, originated at center of hood opening
y	coordinate along direction of cross draft, originated at center of hood opening
z	coordinated normal to x and y coordinates, originated at center of hood opening
ν	kinematic viscosity of air
ξ	distance in x direction from y axis to lower limit of capture envelope
ζ	distance in x direction from origin to intersection of hood centerline and dividing streamline
γ	distance from center of hood opening to stagnation point of dividing streamline

In this study, systematic experiments were conducted to probe flow characteristics of a flanged circular hood in various suctions and cross drafts. Streak patterns obtained from the smoke-trajectory flow visualization method were employed to clarify the variations of flow field. The velocities were measured with a two-component laser Doppler anemometer. The streamline patterns were then obtained from the measured velocity data. The boundary of the effective capture envelope is thus described by a dividing streamline that attains a stagnation point on the y-z plane. The dividing streamlines were normalized by the diameter of the hood opening so that the parameters for hood design become universal.

EXPERIMENTAL ARRANGEMENTS

Supply System of Cross Draft

The experiments were conducted in a system including a hood model, a wind tunnel, peripheral devices, and instruments for measurements, as shown in Figure 1. To employ the laser Doppler velocimeter to measure the velocity field, the cross draft was supplied by an open-loop wind tunnel, as shown in Figure 1, so that the seeding particles for laser-light scattering could be exhausted to the exterior environment. The $50 \times 50 \times 120$ cm test section was made of transparent acrylic plates so that the laser beams could shoot through. Since the velocity of the cross draft is usually low in practical use, the flow velocity in the wind-tunnel test section was regulated by a frequency inverter to values lower than 2 m/sec in this study. Because of the open-loop and low-speed operation, the flow velocity in the test section was very sensitive to the convection current in the exterior environment. To avoid the influence of exterior convection current, the exhaust section of the wind tunnel was specially designed so that stable operation in a range between 0.1 and 20.0 m/sec could be conducted at large exterior convection gusts. In fair weather, the lower limit could be lowered to 0.05 m/sec.

A hot-wire anemometer calibrated by a laser Doppler velocimeter was used to measure and monitor the free-stream velocity of

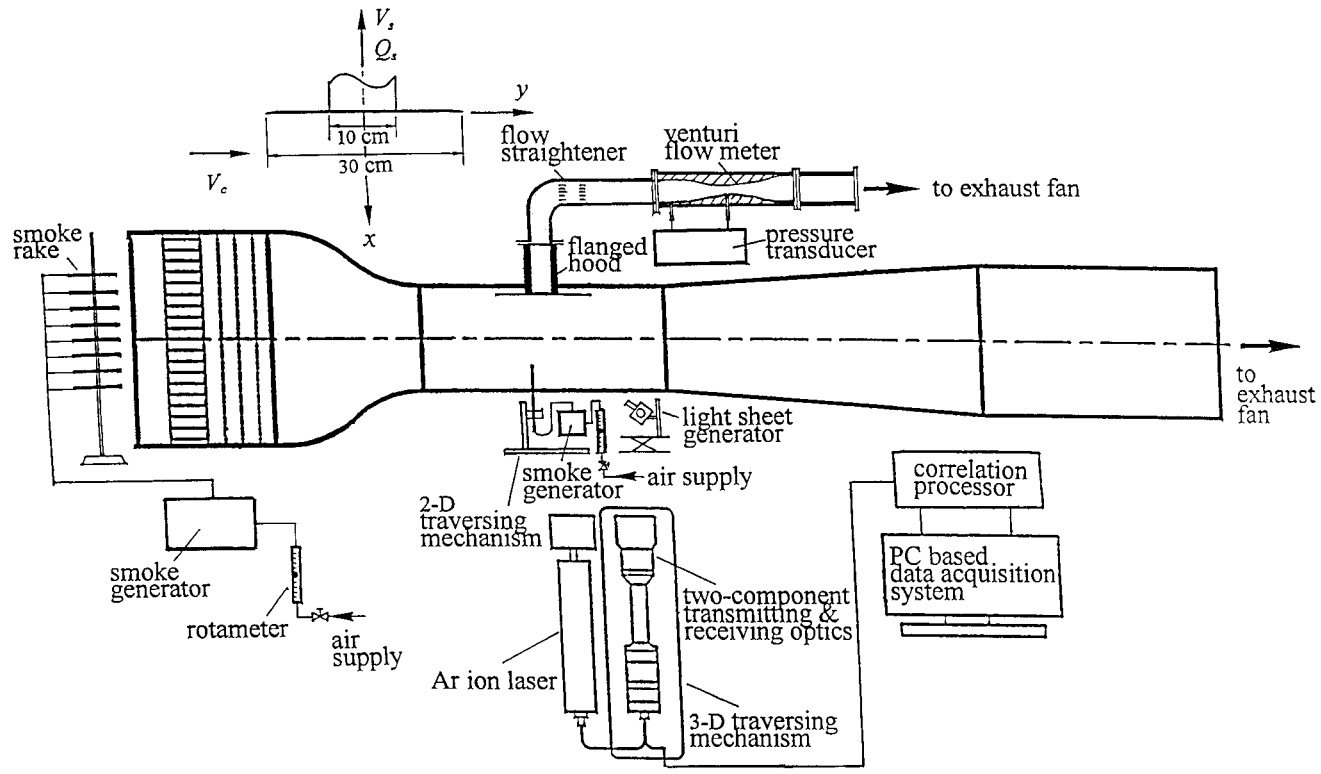

FIGURE 1. Experimental setup

TABLE I. Properties of LDV System

	Green	Blue
Wave length	514.5 nm	488 nm
Focus length of front lens	500 mm	500 mm
Diameter of laser beam waist before expansion	1.0 mm	1.0 mm
Beam intersection angle	12.6°	12.6°
Diameter of focused laser beam	0.075 mm	0.071 mm
Fringe separation	2.34 μm	2.22 μm
Fringe number	32	32
Optical shift frequency	40 MHz	40 MHz
Measuring volume dimensions ($\delta_x \times \delta_y \times \delta_z$)	0.075 × 0.075 × 0.680 mm	0.071 × 0.071 × 0.645 mm

the cross draft. The accuracy of the free-stream velocity measurement was about 0.5% of the reading. The turbulence intensity was less than 0.40% when the wind velocity, V_c, was greater than 1.2 m/sec. The turbulence intensity increased with the decrease of wind velocity when V_c was less than 1.2 m/sec; for example, the turbulence intensity was 0.85% at V_c = 0.4 m/sec. Different turbulence intensities in the cross draft may induce different dispersion effects and lead to different capture efficiency. Because the current subject of study was similar to the analogous case of the aspiration of air from a moving free stream into an aerosol sampler, some experimental results of the aerosol sampler by other investigators can be used for reference. Vincent[10] reported that no systematic variation in mean flow pattern for turbulence ranging in scale from substantially less than to substantially greater than the diameter of an aerosol sampler body with intensity as high as 15% was observed. Therefore, the capture envelope and characteristic quantities obtained from the time-averaged streamlines of the flow field of the suction hood in a cross draft would not be influenced significantly by the free stream turbulence.

Hood and Suction System

The hood model was an acrylic tube with an inner diameter D = 10.0 cm, outer diameter 10.5 cm, and length 50 cm. One end of the tube served as the hood opening. A sharp-edged acrylic square plate was attached on the plane of opening, which served as the flange to decrease the influence of the boundary layer. The width and thickness of the flange were 30 cm and 0.4 cm, respectively. The hood model was installed in the center of the test section and protruded perpendicularly through the ceiling plate 4 cm down into the test section. Positions are described in terms of a rectangular coordinate system (x, y, z) as shown in the upper left corner of Figure 1. Suction of the hood was provided via a set of AC motor/centrifugal fans. The suction flow rate was measured by a venturi flow meter along with an electronic pressure transducer. The accuracy of the suction flow rate measurement is less than 1% of the reading. The operating suction flow rate, Q_s, was between 0.042 and 0.079 m^3/sec. Therefore, the volumetric averaged suction velocity, V_s, at the hood opening was between 5.3 and 10.1 m/sec, corresponding to a suction Reynolds number, Re_s, between 3.53×10^4 and 6.73×10^4.

TABLE II. Statistics of Measurements

	Re_s		
	3.53×10^4	4.84×10^4	6.73×10^4
Re_c		R	
0.27×10^4	0.075		
0.33×10^4	0.094		0.050
0.53×10^4	0.150	0.110	0.079
0.67×10^4	0.188	0.138	0.099
1.00×10^4	0.282		0.149
1.33×10^4	0.377	0.276	0.198

Laser-Light Sheet Flow Visualization System

The laser beam from an argon-ion laser was transmitted through an optical fiber and connected to a 20° laser-light sheet expander. The laser-light sheet expander was mounted on an adjustable block so that the light sheet could be aligned on different planes. The laser-light sheet was adjusted to a thickness of about 0.5 mm and aligned on the symmetry plane z = 0. Mineral oil mist was seeded continuously through a homemade smoke generator into the test section to scatter the laser light. The diameter of the oil mist particles, measured by a Malvern 2600C particle analyzer, was 1.7 ± 0.2 μm. The density was 0.821 g/mL. Ignoring the effect of turbulent diffusion, the relaxation time constant was estimated to be less than 7.7×10^{-5} sec and the Stokes number was on the order of 10^{-6} within the range of experiment. Therefore, the seeding particles could properly follow the flow fluctuations at least up to 10 kHz.[13] The particle images were recorded by a Minolta® Dynax® 9xi still camera. The camera was equipped with an asynchronous variable electronic shutter, ranging from 1/12000 to 30 sec.

Laser Doppler Velocimeter

The velocity field was measured with a two-component laser Doppler velocimeter (LDV). The primary configurations of the LDV system are listed in Table I. The blue and green laser beams were separated, split, and focused through a fiber optical system. The measuring volume dimensions of the green and blue components were 0.075 × 0.075 × 0.680 mm and 0.071 × 0.071 × 0.645 mm, respectively. The fringe separations of green and blue components were 2.34 and 2.22 μm, respectively. The system was configured for backward scattering. A Bragg cell was included in the system for direction identification. The mineral oil mist with average diameter of 1.7 ± 0.2 μm was seeded into the wind tunnel via the smoke rake, as shown in Figure 1. Each velocity data record consists of 3000 samples, each for about 2 sec. The average sampling rate was about 1.5 kHz. The accuracy of the velocity measurement is estimated to be less than 0.5% of the reading.

RESULTS AND DISCUSSION

The Reynolds numbers of the hood suction and cross draft for the experiments, which are determined by the general conditions under which an exterior hood may operate at the work site, are shown in Table II. Three sets of suction Reynolds numbers,

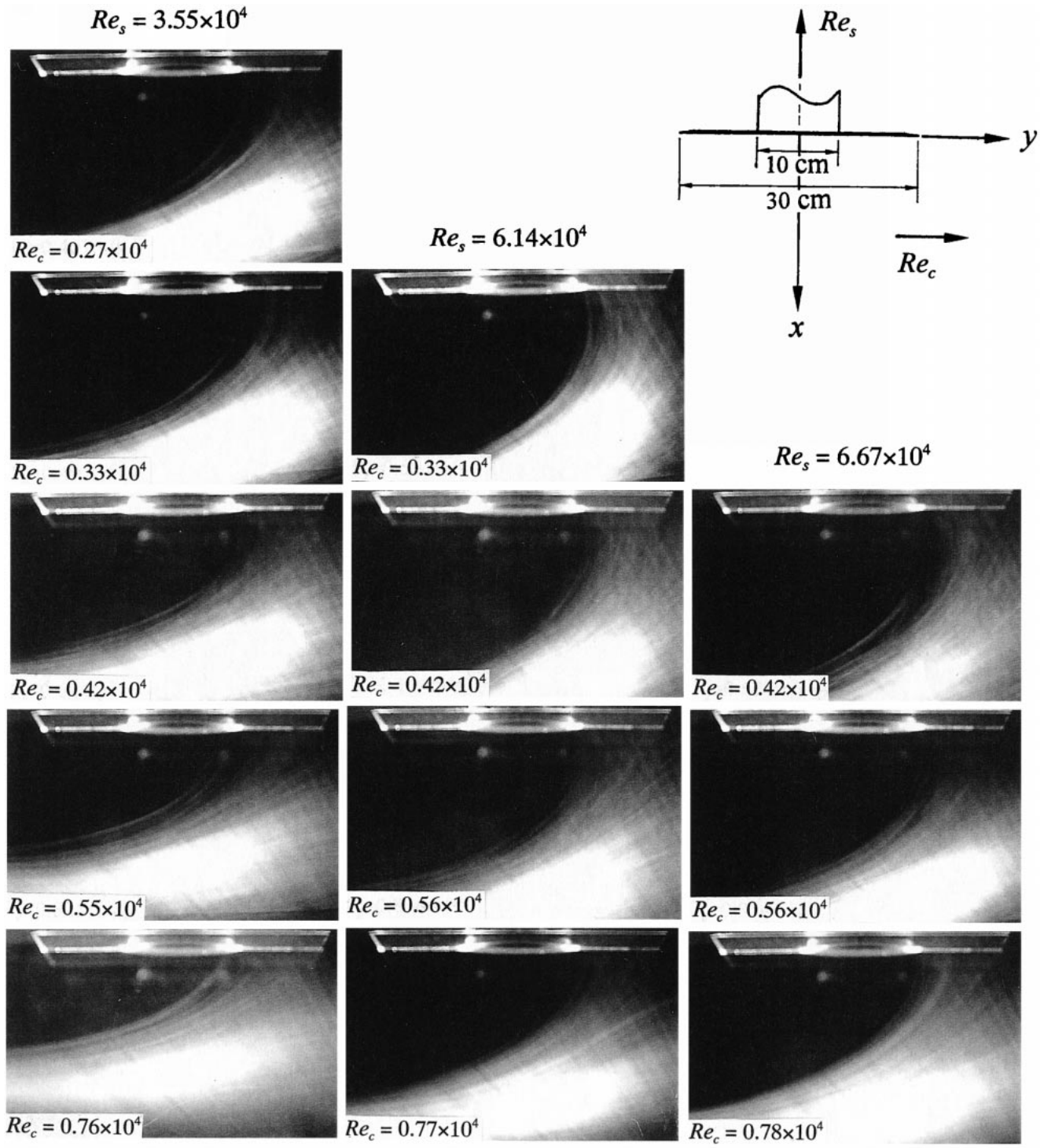

FIGURE 2. Capture envelopes observed by smoke streaks flow visualization method; exposure time 30 sec

$Re_s = 3.53 \times 10^4$, 4.84×10^4, and 6.73×10^4, were conducted in this study. The experimental range of cross draft Reynolds numbers, Re_c, covers from 0.27×10^4 to 1.33×10^4.

Smoke-Streak Patterns

The pictures taken with long exposure shown in Figure 2 were obtained using the laser-light sheet flow visualization method. The smoke was released by a small stainless tube with a diameter of 5 mm. The exit velocity of the smoke stream was set under the isokinetic condition to make the disturbance on the free stream as small as possible. The stainless tube was placed on the symmetry plane, upstream of the test section, and aligned in the direction of free stream. Before the picture was taken, the smoke releasing tube was moved along x direction by a traversing mechanism to a position where the upper streak line of the smoke evolved into the downstream edge of the hood opening. The dark zones in the

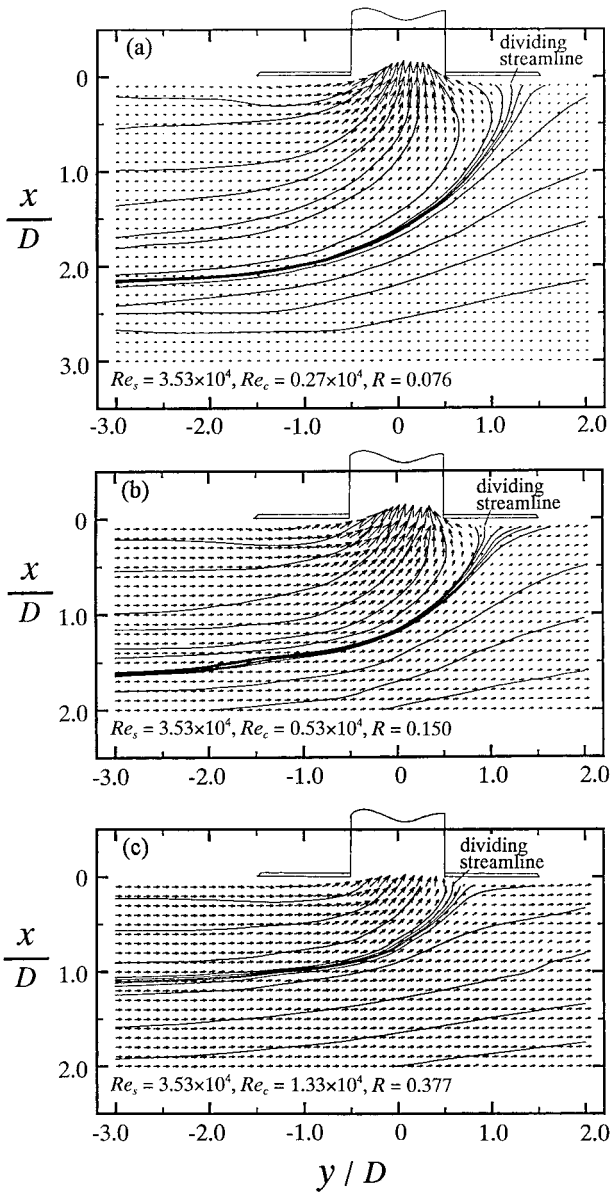

FIGURE 3. Velocity vectors and streamlines measured by LDV. Re_s = 3.53 ×10⁴, (Re_c, R) = (a) Re_c = 0.27 × 10⁴, R = 0.076; (b) Re_c = 0.53 × 10⁴, R = 0.150; (c) Re_c = 1.33 × 10⁴, R = 0.377

pictures of Figure 2 show the capture envelope, and the white regions delineate the smoke streaks outside the capture envelope.

All the capture envelopes in Figure 2 enclosed the hood opening and presented the shape of a half-Rankine nose.[8,9] The farthest point of the capture envelope in the y direction was on the flange and downstream of the hood opening. When the cross-draft Reynolds number, Re_c, was increased at a constant Re_s, the farthest point of the capture envelope on the flange moved back toward the hood opening. The lower boundary of the capture envelope was raised to a level closer to the hood opening, as shown in the pictures of the same column of Figure 2. It is apparent that the capture envelope shrank with the increase of cross draft at a constant suction rate. However, the effect of the suction rate was positive: the capture envelope enlarged with the increase in suction

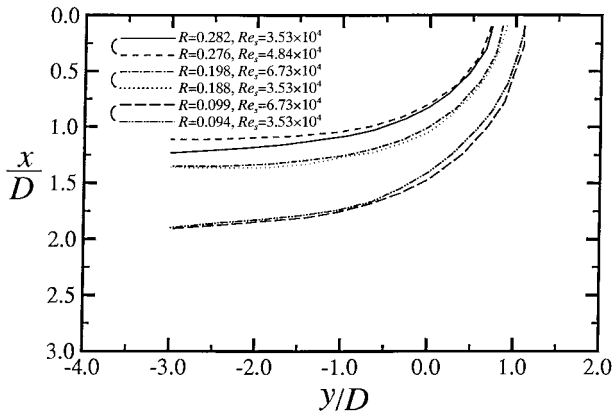

FIGURE 4. Comparisons of dividing streamlines at similar velocity ratios

rate, as shown in the pictures in the same row of Figure 2. Therefore, a contaminant source originally placed in the designed capture zone of an exhaust hood may go beyond the capture envelope, which leads to a failure in hood performance when the hood is attacked by a cross draft.

Capture Envelope and Dividing Streamline

To obtain quantitative and detailed information of the flow field, the two-component LDV was used to measure the velocity distributions on the symmetry plane. Table II shows the range of measurements. A total of 14 flow fields at different Re_s/Re_c combinations were measured. In terms of the velocity ratio $R \equiv V_c/V_s$, the experimental range was $0.05 < R < 0.4$. Different pairs of Re_s and Re_c may give similar values of R so that comparisons based on similar R are possible.

Figure 3a shows the velocity-vector fields and streamline patterns at R = 0.076 and $Re_s = 3.53 \times 10^4$. The velocity vectors near the hood opening have a larger x component. The y component is large when far away from the opening. A streamline (denoted by "dividing streamline") evolves far from upstream at (x/D, y/D) ≈ (2.2, −3.0), which rises up and hits perpendicularly to the flange at (x/D, y/D) ≈ (0.0, 1.2) to form a stagnation point. In the upper left part of the flow field, all the streamlines evolving from upstream lead to the hood opening and construct a capture envelope. The flows near the stagnation point inside the capture envelope even reverse due to the suction effect. Theoretically, all the contaminants inside the capture envelope should follow the flow and be attracted into the hood opening if the dispersion effect is ignored.

Figures 3b and 3c show the velocity vectors and streamline patterns at R = 0.150 and 0.377, respectively. The capture envelope apparently shrinks with the increase of the velocity ratio R; for example, the lower limit of the dividing streamline reduces to x/D ≈ 1.1 and the stagnation point on the flange moves to y/D ≈ 0.65 at R =0.375, as shown in Figure 3c.

Figure 4 shows the dividing streamlines at various cross-draft/suction velocity ratios. The dividing streamlines rise to a higher level with the increase of R. The dividing streamlines at similar values of R almost coincide with each regardless of the velocities of cross draft and suction. It is apparent that the cross draft-to-suction velocity ratio R is a nondimensional parameter that primarily dominates present flow field.

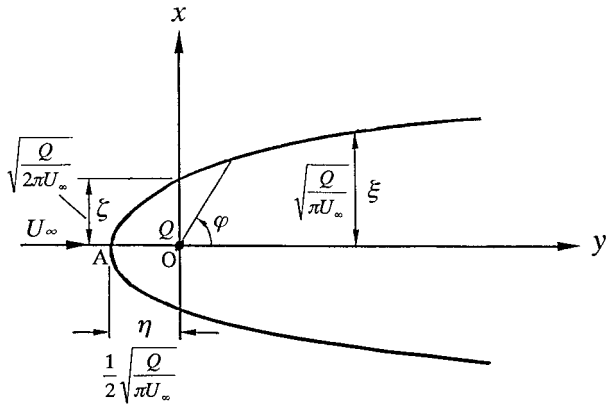

FIGURE 5. Rankine body-of-revolution formed by superimposing a rectilinear flow to a point source

Justification and Correlation

According to the classical potential theory[8,9] of a point source with a strength Q superimposed by a rectilinear flow with a velocity U_∞, a Rankine body-of-revolution is formed, as shown in Figure 5. The streamline passing through the stagnation point A and along $\varphi = \pi$ is written

$$x^2 = \frac{Q}{2\pi U_\infty}(1 + \cos\varphi) \tag{1}$$

Equation 1 is the dividing streamline separating the inner part of Rankine body-of-revolution and outer free streams. The distance between stagnation point A and the source point O is given by

$$\eta = \sqrt{\frac{Q}{4\pi U_\infty}} \tag{2}$$

The distance between source point O and the intersection of the dividing streamline and x axis ($\varphi = \pi/2$ and $y = 0$) is

$$\zeta = \sqrt{\frac{Q}{2\pi U_\infty}} \tag{3}$$

The distance between y axis and the dividing streamline at $\varphi = 0$ and $y \to \infty$ is

$$\xi = \sqrt{\frac{Q}{\pi U_\infty}} \tag{4}$$

If the point source is replaced by a point *sink*, the Rankine body-of-revolution will be reflected about the x axis, that is, the plus sign in Equation 1 should be replaced by a minus sign. If the half Rankine body-of-revolution derived from the model of point sink plus rectilinear flow is adopted to simulate the capture envelope of present flow field, then Equations 1–4 can be modified and used to correlate the current experimental data as follows. If the rectilinear flow velocity U_∞ is replaced by the cross-draft velocity, V_c, and the strength Q of the point sink is replaced by the hood suction rate $Q_s = V_s(\pi D^2/4)$ the equation of dividing streamline in nondimensional form then becomes

$$\frac{x}{D} = \frac{0.3536}{\sqrt{R}}\sqrt{\left(1 - \frac{\frac{y}{D}}{\sqrt{\left(\frac{x}{D}\right)^2 + \left(\frac{y}{D}\right)^2}}\right)} \tag{5}$$

From Equation 2, the distance η between the stagnation point and the point sink becomes

$$\eta = \sqrt{\frac{V_s\frac{\pi D^2}{4}}{4\pi V_c}} = \frac{\frac{D}{4}}{\sqrt{R}}$$

That is, in nondimensional form,

$$\frac{\eta}{D} = \frac{0.25}{\sqrt{R}} \tag{6}$$

From Equation 3, the lower limit of the dividing streamline on the central line is

$$\zeta = \sqrt{\frac{V_s\frac{\pi D^2}{4}}{2\pi V_c}} = \frac{D}{2\sqrt{2}\times\sqrt{R}}, \quad \text{or} \quad \frac{\zeta}{D} = \frac{0.3536}{\sqrt{R}} \tag{7}$$

From Equation 4, the distance ξ in x direction from the y axis to the lower limit of the capture envelope is written as

$$\xi = \sqrt{\frac{V_s\frac{\pi D^2}{4}}{\pi V_c}} = \frac{\frac{D}{2}}{\sqrt{R}}, \quad \text{or} \quad \frac{\xi}{D} = \frac{0.5}{\sqrt{R}} \tag{8}$$

It is apparent that in Equations 5–8 the nondimensional equations of the dividing streamline and characteristic lengths are all functions of $1/\sqrt{R}$. However, in practical use, the coefficients and function type in Equations 5–8 are expected to be modified because (1) the hood has a finite suction opening instead of a point sink, (2) the fluid is not inviscid even though the viscosity is small, and (3) the dispersion effect is not completely negligible.

If the least squares method is employed to regress the experimental data, the nondimensional equations are obtained as follows Dividing streamline:

$$\frac{x}{D} = \frac{0.44}{\sqrt{R}}\sqrt{\left(1 - \frac{\frac{y}{D}}{\sqrt{\left(\frac{x}{D}\right)^2 + \left(\frac{y}{D}\right)^2}}\right)} \tag{9}$$

Characteristic lengths:

$$\frac{\eta}{D} = \frac{0.4285}{R^{0.4135}} \tag{10}$$

$$\frac{\zeta}{D} = \frac{0.4073}{R^{0.5533}} \tag{11}$$

$$\frac{\xi}{D} = \frac{0.6216}{R^{0.4924}} \tag{12}$$

The exponent -0.5 in the general function type $1/\sqrt{R}$ for the dividing streamline and characteristic lengths in the theoretical Equations 6–8 is modified a little by ± 0.1 in the empirical Equations 10–12. However, the coefficients in the empirical equations deviate much from theoretical values by 15 to 71%. The total effects induced by finite opening, viscosity, and dispersion are lumped in the correlated equations by modifying the coefficients and function type.

Figure 6 shows the comparisons of the dividing streamlines among the experimental results, theoretical Equation 5, and correlation Equation 9 at various R. Correlated Equation 9 fits the experimental results in a maximum deviation less than 10%, which is generally acceptable for the purpose of hood design. In the area

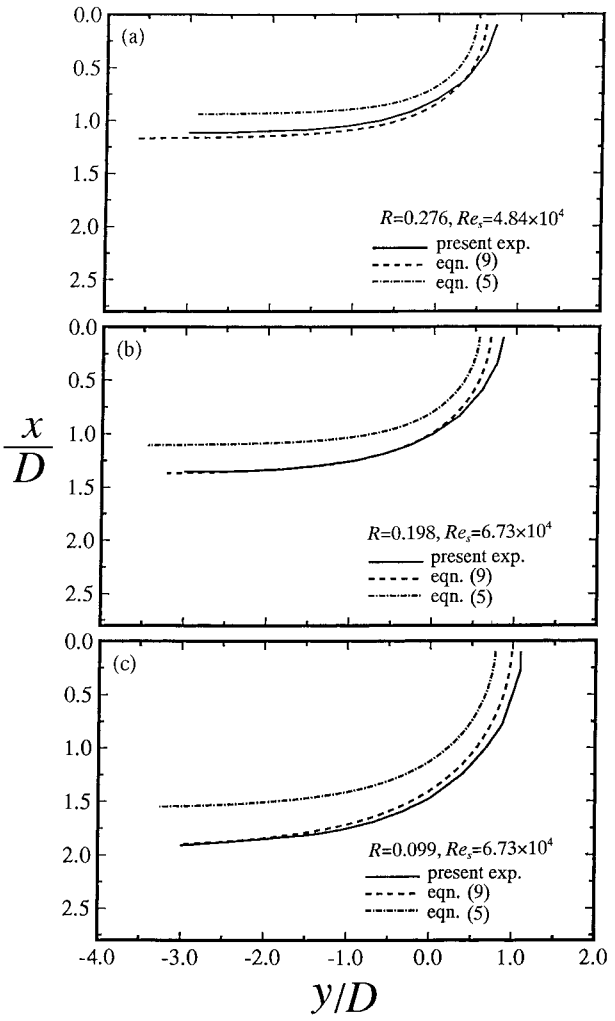

FIGURE 6. Comparisons of dividing streamlines among results of experimental results, point-sink potential flow theory, and correlation

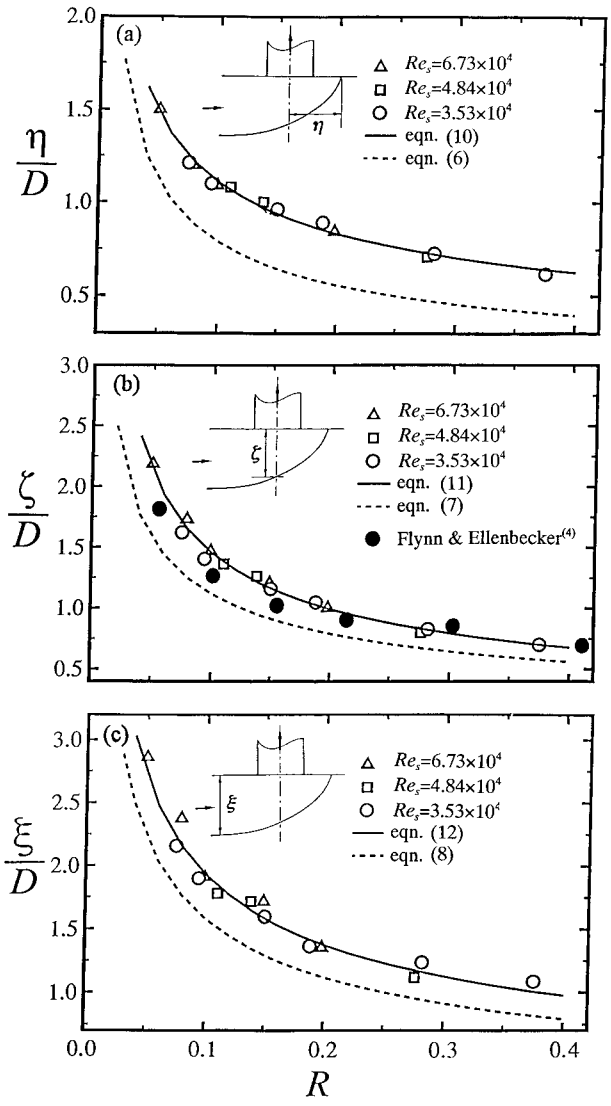

FIGURE 7. Comparisons of characteristic lengths among results of experimental results, point-sink potential flow theory, and correlation

under the hood opening, that is, $-1/2 < y/D < 1/2$, the deviation is less than 3%. Since the location and movement of the contaminant sources usually are limited within the projection of the hood opening, the error induced by the deviation of fitting is insignificant. However, theoretical Equation 5 of the point sink potential flow theory predicts a smaller capture envelope. The finite opening has a positive effect on magnifying the capture capability.

Figure 7 shows the comparisons among the experimental data, theoretical Equations 6–8, and correlation Equations 10–12 at various R. The theoretical results apparently underestimate the real situations. The function type of the parameter ξ/D—that is, the normalized distance in x direction from the y axis to the lower limit of the capture envelope—does not deviate much from $R^{-0.5}$. However, the parameters η/D and ζ/D deviate from the theoretical function type $R^{-0.5}$ in different ways. The exponents -0.4135, -0.5533, and -0.4924 in Equations 10, 11, and 12, respectively, justify the difference.

The ζ/D data measured by Flynn and Ellenbecker[4] using the aerosol sampling technique are incorporated in Figure 7b for comparison. Three hood diameters, D = 5.25, 10.226, and 15.405 cm, and various velocity ratios, R, ranging from 0.082 to 0.415, were employed in their experiments. They suggested that the critical distance ζ/D can be obtained at 50% mean capture efficiency. The symbol ● in Fig 7b represents the data interpolated from the dimensionless axial distance listed in the Table I of Flynn and Ellenbecker.[4] Very fair agreements are observed between the present experimental results and the results of Flynn and Ellenbecker's aerosol concentration sampling. Both techniques are eligible for the evaluation of the characteristic length scales of the hood performance.

Extension to Different Opening Sizes

The previously discussed results were obtained from the experimental data of a hood model with a suction opening diameter of 10 cm. Although the theoretical justification of the nondimensional equations explains the applicability in different hood diameters, no other experimental results agree with this explanation. To the extent that Equations 9–12 apply to different opening diameters, the computational results derived from the finite-opening

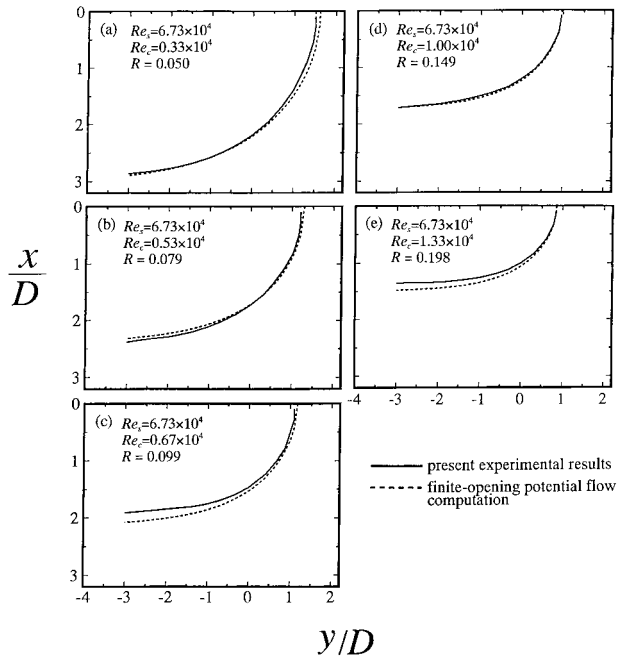

FIGURE 8. Comparisons of dividing streamlines between experimental results and finite-opening potential flow theory

potential flow theory[6,11] are employed for comparison. The finite-opening potential flow computational method deals with an inviscid, irrotational flow. By assuming a uniform normal velocity at the hood opening (precisely, a uniform potential gradient there), the exhaust velocity is determined by integration of uniformly distributed sinks on the hood opening. The flow velocity then is given by superimposing the exhaust velocity on the cross-draft velocity. A streamline can be determined by a Runge-Kutta integration[14] about a Lagrangian equation.[11]

Figure 8 shows comparisons between the present measurements and the finite-opening potential flow theory[6,11] at D = 10 cm and various R. Apparently, the computational results deviate from the experimental data in a tolerable range. The maximum deviation is about 9% in x/D and 8% in y/D. Several factors may contribute to the deviation between the computational and experimental results. In the finite-opening potential flow computation the assumption of uniform velocity at the opening does not hold true in the real flow. Also, the viscosity and its associated effects, such as the boundary layer induced on the flange, nonsingularity at the edge of the opening, turbulent dispersion effect, and so forth, may cause deviation between measurements and computations.

Figure 9 shows the comparisons between the computational results of the finite-opening potential flow theory[11] at D other than 10 cm and the experimental results at D = 10 cm at various R. All experimental and computational results fall in a narrow band, which is far from the results of the point sink theory. The characteristic lengths in Figure 10 also show the correspondence of various sizes of the hood opening. Therefore, the applicability of Equations 9–12 to different hood opening diameters should be appropriate.

Application Guidelines

Equations 9–12 set up the foundations for the design of the exterior flanged exhaust hood. The following arguments provide the guidelines for application.

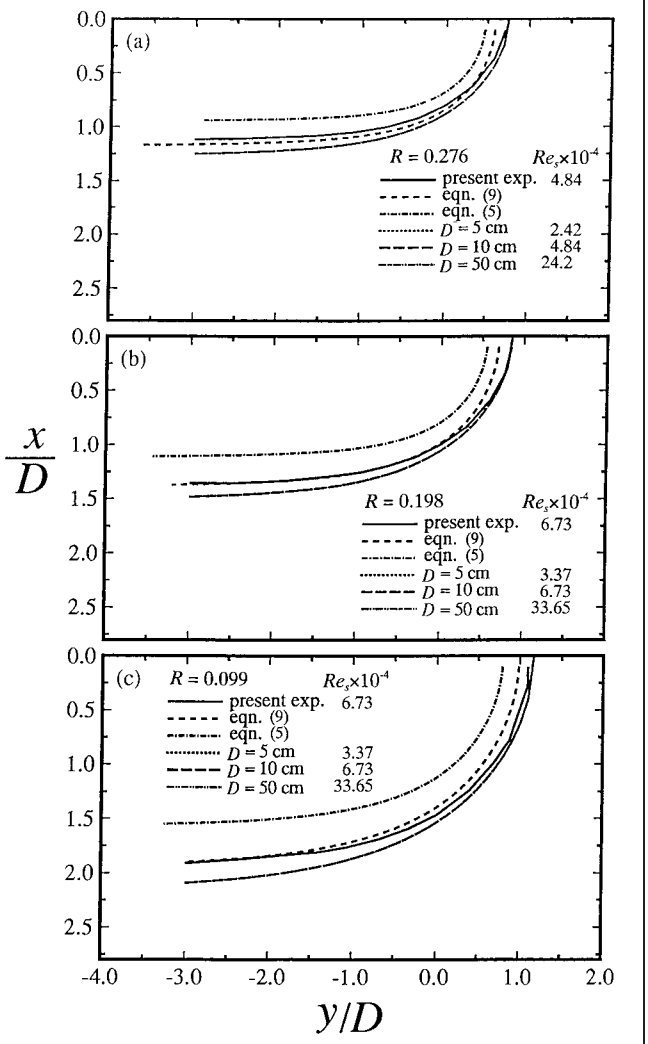

FIGURE 9. Comparisons of dividing streamlines among results of experimental results, point-sink potential flow theory, finite-opening potential flow theory, and correlation at various hood opening diameters

- Equation 9 of the dividing streamline provides complete information for the capture envelope under designated R and D.
- Equation 10 of the distance η enables the designer to calculate minimum required flange size under designated R and D.
- Equation 11 of the distance ζ provides the installing range of the contaminant source on the center line. Contaminant sources often are installed on the center line under a hood, so Equation 11 offers a quick estimation for this application under designated R and D.
- Equation 12 of the distance ξ provides the estimation of the off-center-line location of the contaminant source under designated R and D.

CONCLUSIONS AND RECOMMENDATIONS

The flow patterns of an exterior circular hood subject to the influence of various uniform cross drafts were phenomenologically and quantitatively studied. The following conclusions are drawn from the results.

By modeling the classical potential theory of the point sink plus

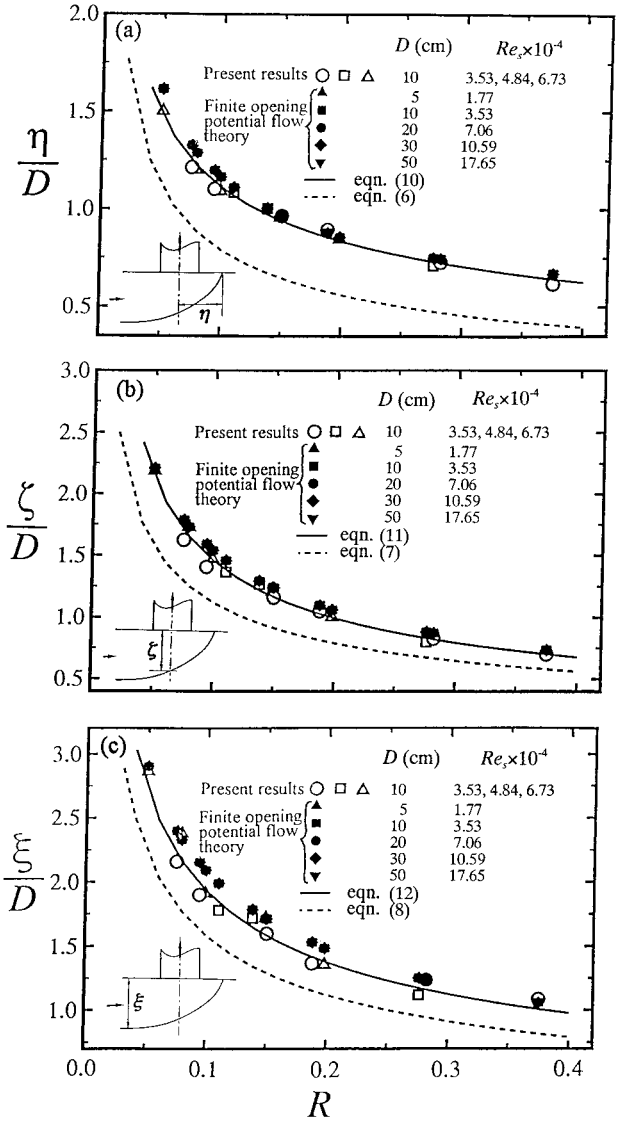

FIGURE 10. Comparisons of characteristic lengths among results of experimental results, point-sink potential flow theory, finite-opening potential flow theory, and correlation at various hood opening diameters

rectilinear flow, the variables dominating the flow characteristics—for example, the normalized geometry of the capture envelope and characteristic lengths—are theoretically justified and correlated to be functions of the cross draft-to-suction velocity ratio, R. The same values of R will give the same geometric characteristics of the capture envelope.

The correlated Equations 9–12 provide quick and convenient tools for the design of a hood with a circular opening and a simple flat flange subject to a steady uniform cross draft. However, the assumption of a steady uniform cross-draft perpendicular to the hood centerline is an idealization. In practical industrial hygiene situations different geometry of hood openings and flanges subject to nonuniform, unsteady, accelerating, cyclonic, or direction-varying cross drafts may be expected. To obtain universal criteria for practical use, more research is required to account for these complicated situations.

The centerline distance of the capture-envelope boundary obtained from the current streamline method is similar to that obtained from the 50% capture efficiency method. However, the streamline method is independent of free-stream turbulence and offers more information for characterizing the geometry of the capture zone, such as the stagnation point, dividing streamline, and so forth. If a quick computation of the effective capture zone is required, the streamline method is a reasonable choice. However, if the capture efficiency is to be evaluated, the concentration measurement is unavoidable.

REFERENCES

1. **Dalla Valle, J.M.:** *Exhaust Hoods.* New York: Industrial Press, 1945. pp. 21–48.
2. **Drkal, F.:** Strömungsverh ältnisse bei runden saug öffnugen mit flansch. *Z. Heiz. Lüft. Klim. Haus. 21*:271–273 (1970).
3. **Flynn, M.R., and Ellenbecker, M.:** Emperical validation of theoretical velocity fields into flanged circular hoods. *Am. Ind. Assoc. J. 48*: 380–389 (1987).
4. **Flynn, M.R., and Ellenbecker, M.:** Capture efficiency of flanged circular local exhaust hoods. *Ann. Occup. Hyg. 30*:497–513 (1986).
5. **Flynn, M.R., and Ellenbecker, M.:** The potential flow solution for airflow into a flanged circular hood. *Am. Ind. Assoc. J. 46*:318–322 (1985).
6. **Flynn, M.R., and Miller, C.T.:** Comparison of models for flow through flanged and plain circular hoods. *Ann. Occup. Hyg. 32*:373–384 (1988).
7. **Heinsohn, R.J.:** *Industrial Ventilation: Engineering Principles.* New York: John Wiley & Sons, 1991. pp. 360–428.
8. **Yuan, S.W.:** *Foundations of Fluid Mechanics.* Englewood Cliffs, N.J.: Prentice Hall, 1967. pp. 224–231.
9. **Currie, I.G.:** *Fundamental Mechanics of Fluids.* New York: McGraw-Hill, 1974. pp. 155–160.
10. **Vincent, J.H.:** *Aerosol Sampling: Science and Practice.* New York: John Wiley & Sons, 1989. pp. 61–85.
11. **Chen, Y.K., W.Y. Yeh, and C.W. Chen:** Theoretical studies on control velocity of flanged circular hood. *Quart. Occup. Medic. Ind. Hyg. 30*:497–513 (1997).
12. **Alenius, S., and A. Jansson:** *Air Flow and Particle Transport into Local Exhaust Hoods—A Verified Computer Model.* Solna, Sweden: National Institute of Occupational Health, 1989. p. 34.
13. **Flagan, R.C., and J.H. Seinfeld:** *Fundamentals of Air Pollution Engineering.* Englewood Cliffs, NJ: Prentice Hall, 1988. pp. 290–357.
14. **Nakamura, S.:** *Applied Numerical Methods with Software.* Englewood Cliffs, NJ: Prentice Hall, 1991. pp. 334–342.